JOURNAL OF SOLID STATE CHEMISTRY 57, 68–81 (1985)

New Ternary and Quaternary Transition-Metal Selenides: Syntheses and Characterization*

DOUGLAS A. KESZLER AND JAMES A. IBERS

Department of Chemistry, Northwestern University, Evanston, Illinois 60201

AND SHANG MAOYU AND LU JIAXI

Fujian Institute of Research on the Structure of Matter, Chinese Academy of Sciences, Fuzhou, Fujian, People's Republic of China

Received June 5, 1984

New ternary and quaternary transition-metal selenides have resulted from substitutional chemistry of the phase $Nb_2Pd_3Se_8$ and examination of the system Nb/Pd/Se. The structures of the phases $Ta_2Pd_3Se_8$, $Co_2Ta_4PdSe_{12}$, and $Nb_2Pd_{0.71}Se_5$ have been established through single-crystal X-ray methods. The compound $Ta_2Pd_3Se_8$ forms in space group *Pbam* with two formula units in a cell of dimensions a = 15.152(2), b = 10.631(2), and c = 3.540(1) Å. This material is isostructural with $Nb_2Pd_3Se_8$. The compound $Co_2Ta_4PdSe_{12}$ forms in space group *C2/m* with two formula units in a cell of dimensions a = 12.951(3), b = 3.413(1), c = 19.277(5) Å, and β = 110.37(2)°. This material forms with a new laminar structural type; each layer is composed of an unusual association of metal-centered Se polyhedra. The Pd atom occupies a square plane, the Co atom occupies a square pyramid and there are two types of Ta atoms—octahedral and trigonal prismatic. The layers pack in a pseudo-closest-packed manner with the formation of several vacant octahedral and tetrahedral sites between the layers. Like the phase $Co_2Ta_4PdSe_{12}$ the compound $Nb_2Pd_{0.71}Se_5$ also forms in a new layered structural type. This compound crystallizes in space group *C2/m* with four formula units in a cell of dimensions a = 12.788(6), b = 3.391(1), c = 15.416(6) Å, and β = 101.48(2)°. The material consists of layers of composition $^2_\infty[Nb_4PdSe_{10}]$ that result from association of Pd-centered Se square planes and Nb-occupied Se trigonal prisms. Between these layers a rhombic site is 42% occupied by an additional Pd atom that bonds to four coplanar Se atoms. The results of electrical conductivity measurements indicate that this material is a metallic conductor.

Introduction

Considerable research in modern solid-state inorganic chemistry is focused on transition-metal materials with partially filled *d*-like conduction bands. Interest in these materials derives from the variety of physical phenomena that arise from these bands: metal–semiconductor transitions, magnetic interactions, superconductivity, strong metal–metal bonding, and charge-density waves. One class of materials where many of these phenomena occur are the binary and ternary chalcogenides of the Group VB transition metals (*1–10*). In the ternary (quaternary) transition-metal mate-

* Presented at the Symposium on Metal–Metal Bonding in Solid State Clusters and Extended Arrays, held during the American Chemical Society meeting, St. Louis, Missouri, April 9–10, 1984.

0022-4596/85 $3.00

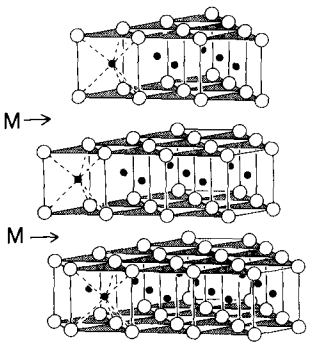

FIG. 1. Schematic representation of M_xNb(Ta)Se_2.

rials two extensive families of compounds have been characterized: M_xNb(Ta)Se_2 (M = Ti, V, Cr, Mn, Fe, Co, Ni, Rh; $x < 0.33$) (*11*), and $MM'Nb_2Se_{10}$ (M = Fe, V, Cr; M' = Fe, V, Cr, Nb) (*12–15*). As shown in Fig. 1, for the former series the ternary atom, M, resides in an octahedral site between layers of Nb(Ta)-occupied edge-shared trigonal prisms of Se atoms. This low-dimensional structural nature is retained for the series $MM'Nb_2Se_{10}$ where the ternary and quaternary atoms occur within the layers. As shown in Fig. 2, the layers are composed of collocated columns of trigonal prismatic chains of $NbSe_3$ bridged by columns of edge-shared Se octahedra occupied by the $M(M')$ atom(s).

In a recent report (*16*) we speculated that new ternary materials (for example, of the Group VB transition metals) should be formed upon introduction of atoms with stereochemical preferences not necessarily consonant with these well-characterized Nb(Ta)–Se substructures. From this speculation resulted the preparation of the new material $Nb_2Pd_3Se_8$ (*16*). This phase forms with a new channel-type structure that contains Nb atoms in a trigonal prismatic environment of Se atoms and two types of Pd atoms—square planar and square pyramidal—each coordinated by Se atoms.

Here we report the syntheses and characterization of three new compounds that are derived from substitutional chemistry on $Nb_2Pd_3Se_8$ and by additional investigation of the Nb/Pd/Se system. The compound $Ta_2Pd_3Se_8$ was prepared in a manner analogous to $Nb_2Pd_3Se_8$ and is isostructural with it. The compound $Co_2Ta_4PdSe_{12}$ arose from an attempt to substitute Co atoms for the five-coordinate Pd atoms in $Ta_2Pd_3Se_8$. Indeed $Co_2Ta_4PdSe_{12}$, which is a new laminar structural type, contains five-coordinate Co atoms. The third new compound to be described is the phase $Nb_2Pd_{0.71}Se_5$, which resulted from a different starting composition in the Nb/Pd/Se system.

Although strong metal–metal bonding is not evident in these materials, the observed metallic conductivity for the phase $Nb_2Pd_{0.71}Se_5$ undoubtedly arises from a partially filled d-like band. As noted previously this characteristic is the *raison d'etre* for the preparation of these materials. In this account then we describe aspects of a new and developing chemistry where the details and nature of the metal–metal interactions await additional study and clarification.

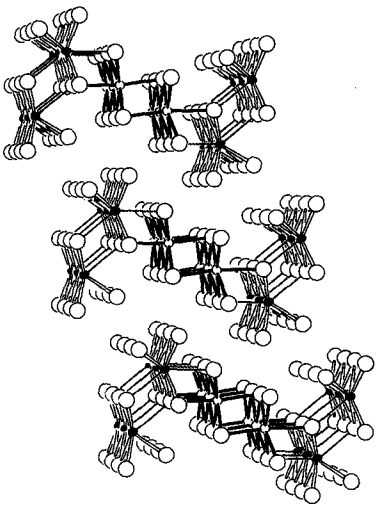

FIG. 2. Drawing of the structural type $MM'Nb_2Se_{10}$ (Ref. (*15*)).

TABLE I

CRYSTAL DATA AND INTENSITY COLLECTION FOR NEW SELENIDES

	$Ta_2Pd_3Se_8$	$Co_2Ta_4PdSe_{12}$	$Nb_2Pd_{0.71}Se_5$
Mol. wt.	1318.78	1907.58	656.16
Space group	D^9_{2h}-*Pbam*	C^3_{2h}-*C2/m*	C^3_{2h}-*C2/m*
a, Å	15.152(2)	12.951(3)	12.788(6)
b, Å	10.631(2)	3.413(1)	3.391(1)
c, Å	3.540(1)	19.277(5)	15.416(6)
α, deg.	90[a]	90[b]	90
β, deg.	90[a]	110.37(2)	101.48(2)
γ, deg.	90[a]	90[b]	90
V, Å^3	570	799	654
Z	2	2	4
T of data collection, K	298	298	115[c]
Crystal vol., mm^3	0.00011	0.00054	0.00032
Crystal shape	Flattened needle, bound by {1$\bar{1}$0}, {001}, ($\bar{1}$30), and (130)	Plate, bound by {20$\bar{1}$}, {001}, and {010}	Rod, bound by {20$\bar{1}$}, {001}, {100}, {010}, and (20$\bar{3}$)
Radiation	Graphite monochromatized Mo$K\alpha$ ($\lambda(K\alpha_1)$ = 0.7093 Å)		
Linear abs. coeff., cm^{-1}	487	571	328
Transmission factors[d]	0.373–0.616	0.031–0.467	0.289–0.446
Detector aperture, mm	Horizontal—2 Vertical—2 + 1.25 tan θ, 20 cm from crystal	Horizontal—4 Vertical—4 + 1.05 tan θ, 20 cm from crystal	Horizontal—5.5 Vertical—3.6, 32 cm from crystal
Takeoff angle, deg.	2.5	4.0	3.2
Scan speed, deg. min^{-1}	2.67 in 2θ ($2° \le 2\theta \le 40°$) 2.29 in 2θ ($40° < 2\theta \le 80°$)	8.0 in 2θ ($2° \le 2\theta \le 40°$) 4.0 in 2θ ($40° < 2\theta \le 84°$)	2.0 in 2θ
Scan range, deg.	1.5 below $K\alpha_1$ to 1.5 above $K\alpha_2$	1.5 below $K\alpha_1$ to 1.5 above $K\alpha_2$	1.0 below $K\alpha_1$ to 1.4 above $K\alpha_2$
λ^{-1} sin θ, limits, Å^{-1}	0.0246–0.9062 $2° \le 2\theta(\text{Mo}K\alpha_1) \le 80°$	0.0246–0.9415 $2° \le 2\theta(\text{Mo}K\alpha_1) \le 84°$	0.0492–0.9969 $4.0° \le 2\theta(\text{Mo}K\alpha_1) \le 90°$
Background counts	$\frac{1}{4}$ of scan range on each side of reflection[e]	$\frac{1}{4}$ of scan range on each side of reflection[e]	10 sec at each end of scan with rescan option[f]
Data collected	$\pm h, \pm k, \pm l$ ($2° \le 2\theta \le 40°$) $\pm h, k, l$ ($40° < 2\theta \le 60°$) h, k, l, ($60° < 2\theta \le 80°$)	$\pm h, \pm k, \pm l$ ($2° \le 2\theta \le 40°$) $h, k, \pm l$ ($40° < 2\theta \le 84°$)	$\pm h, \pm k, \pm l$ ($4° \le 2\theta \le 30°$) $\pm h, k, l$ ($30° < 2\theta \le 90°$)
p factor	0.06	0.04	0.04
No. unique data, including $F_0^2 < 0$	1976	3124	2359
No. unique data with $F_0^2 > 3\sigma(F_0^2)$	1262	1878	2053
$R(F^2)$	0.135	0.149	0.079
$R_w(F^2)$	0.084	0.173	0.102
R (on *F* for $F_0^2 > 3\sigma(F_0^2)$)	0.033	0.054	0.050
Error in observation of unit wt, e^2	0.90	1.96	1.58

[a] Refinement of the cell parameters α, β, and γ affords the values 90.00(2), 90.01(2), and 90.00(1)°, respectively.
[b] Refinement of the cell parameters α and γ affords the values 90.03(2) and 89.97(2)°, respectively.
[c] The low-temperature system is based on a design by J. C. Huffman, Ph.D. thesis, Indiana University, 1974.
[d] The analytical method as employed in the Northwestern absorption program, AGNOST, was used for the absorption correction (J. de Meulenaer and H. Tompa, *Acta Crystallogr.* **18**, 1035, 1965).
[e] Reflections with $\sigma(I)/I > 0.33$ were rescanned.
[f] The diffractometer was operated under the Vanderbilt disk oriented system (P. G. Lenhert *J. Appl. Crystallogr.* **8**, 568, 1975).

Experimental

$Ta_2Pd_3Se_8$. The stoichiometric combination of the elements, Ta powder (ALFA, 99.9%), Pd powder (AESAR, 99.9%), and Se powder (ATOMERGIC, 99.999%) was thoroughly ground and placed in a silica tube, which was then evacuated and sealed. The charge was heated at 1000 K for 10 days with intermediate grindings every 3 days. After the final period of heating, bromine (~2 mg/cm^3 of tube volume) was added to the contents of the tube. The vessel was then placed for 3 weeks in a furnace having a temperature gradient of 1000–900 K. Small needle-shaped crystals formed at the hot end of the tube. The presence of the three elements in these crystals was confirmed by qualitative analysis with the electron microprobe of an EDAX-equipped Cambridge S4 scanning electron microscope.

Analysis of preliminary oscillation and Weissenberg photographs revealed that the crystals belong to the Laue group *mmm*. The systematic absences ($h0l$, $h = 2n + 1$; $0kl$, $k = 2n + 1$) are indicative of the space groups $C_{2v}^8 - Pba2$ and $D_{2h}^9 - Pbam$. As a satisfactory agreement index of 0.01 results from averaging, after correction for absorption, of the Friedel pairs for the complete inner sphere of data, the centric group *Pbam* is favored. The lattice constants were determined from least-squares analysis of 25 automatically centered reflections in the range $26° < 2\theta$ (Mo$K\alpha_1$) $< 35°$ on an Enraf-Nonius CAD4 diffractometer. Six standard reflections monitored every 3 hr exhibited no significant fluctuation or decay during the course of data collection. Crystal data and other crystallographic details are summarized in Table I.

All calculations were performed on a Harris 800 computer with programs standard for this laboratory (*17*). Conventional atomic scattering factors (*18*) were used and anomalous dispersion corrections (*19*) were applied to each atom with values $\Delta f'$ and $\Delta f''$ from Cromer and Waber (*18*). These values are also used in all succeeding calculations. Since the X-ray diffraction pattern of powdered crystals was in satisfactory agreement with a pattern calculated from the positional parameters of the known structure of $Nb_2Pd_3Se_8$ (*16*), the initial atomic parameters for $Ta_2Pd_3Se_8$ were derived from this phase. After an absorption correction data equivalent in space group *Pbam* were averaged. The final cycle of refinement performed on F_0^2 with all 1976 unique reflections afforded the residuals 0.135 and 0.084 for R and R_w, respectively. An analysis of F_0^2 as a function of F_0^2, λ^{-1} sin θ, and Miller indices revealed no unusual trends. No peaks with height greater than 2% of a Ta atom were observed in the final difference electron density map.

Final atomic parameters are provided in Table II. Anisotropic thermal parameters and structure amplitudes are given in Tables S-I and S-II,[1] respectively.

$Co_2Ta_4PdSe_{12}$. A combination of the elements, Co powder (ALFA, 99.8%), Ta powder (ALFA, 99.9%), Pd powder (AESAR, 99.9%), and Se powder (ATOMERGIC, 99.999%), was heated in a sealed, evacuated (ca. 10^{-5} Torr) silica tube for 10 days with intermediate grindings every 3 days. Bromine (~2 mg/cm^3 of tube volume) was then added to the contents of the tube and the vessel placed for 3 weeks in a tube furnace having a temperature gradient of 1000–900 K. Several platelet-shaped crystals formed at the hot end of the tube. The presence of the four elements in these crystals was confirmed by an electron microprobe analysis.

[1] See NAPS Document No. 04240 for 31 pages of supplementary materials from ASIS/NAPS, Microfiche Publications, P.O. Box 3513, Grand Central Station, New York, New York 10163. Remit in advance $4.00 for microfiche copy or $9.95 for photocopy. Outside the U.S. and Canada add $1.50 for microfiche postage or $6.50 for photocopy postage. All orders must be prepaid.

TABLE II

POSITIONAL PARAMETERS AND EQUIVALENT ISOTROPIC THERMAL PARAMETERS FOR $Ta_2Pd_3Se_8$

Atom	Wyckoff notation	Site symmetry	x	y	z	B_{eq}[a] (Å^2)
Ta	4*h*	*m*	0.116831(22)	0.215420(33)	½	0.6
Pd(1)	2*a*	2/*m*	0	0	0	0.9
Pd(2)	4*g*	*m*	0.216148(41)	0.379862(61)	0	0.7
Se(1)	4*g*	*m*	0.990815(54)	0.230843(80)	0	0.8
Se(2)	4*g*	*m*	0.156373(53)	0.043836(78)	0	0.7
Se(3)	4*h*	*m*	0.283187(55)	0.249182(89)	½	0.8
Se(4)	4*h*	*m*	0.115607(59)	0.455457(84)	½	0.9

[a] $B_{eq} = \frac{4}{3}\sum_i \sum_j \beta_{ij}(\hat{a}_i \cdot \hat{a}_j)$ here and in succeeding tables.

Analysis of oscillation and Weissenberg photographs revealed that the crystals belong to the monoclinic system. The systematic extinction (*hkl*; $h + k = 2n + 1$) is indicative of the space groups $C_2^3 - C2$, $C_s^3 - Cm$, and $C_{2h}^3 - C2/m$. The centric group $C2/m$ is favored by the satisfactory agreement index 0.02 obtained from averaging the absorption-corrected intensities of the Friedel pairs for the inner set of data ($2° \leq 2\theta$ (Mo$K\alpha_1$) $\leq 40°$). The refined cell parameters and additional crystal data are given in Table I.

Intensity data were collected with the ω-2θ technique on an Enraf-Nonius CAD4 diffractometer. During the course of data collection, anomalously high background counts were observed for several reflections of the class *h*0*l*. The high counts resulted from overlap of adjacent strong reflections. The intensity data for this class of reflections were subsequently recollected with the ω-scan technique. The scale factor for merging the two sets of data was derived as the average ratio of 288 reflections with $F_0^2 > 3\sigma(F_0^2)$ from each set of data. Six standard reflections, measured every 3 hr, showed no significant variation in intensity throughout the data collection.

Initial calculations were performed on a VAX 11/730 computer with the use of the Enraf-Nonius CAD4-SDP programs (*20*). By examination of an E map all the atoms were located except Co, Se(5), and Se(6). These remaining atoms were located from ensuing electron density maps. All subsequent calculations were performed on a Harris 800 computer with programs and methods standard for this laboratory (*17*). The final cycle of refinement performed on F_0^2 with anisotropic thermal parameters for each atom resulted in the residuals 0.149 and 0.173 for R and R_w, respectively. An analysis of F_0^2 as a function of F_0^2, $\lambda^{-1} \sin \theta$, and Miller indices exhibited no unusual trends. The final electron density map revealed no features greater than 2.5% of the height of a Ta atom.

The final positional and equivalent isotropic thermal parameters are given in Table III. Final anisotropic thermal parameters and structure amplitudes are provided in Tables S-III and S-IV,[1] respectively.

$Nb_2Pd_{0.71}Se_5$. The single crystals characterized in this investigation were obtained from a combination of the elements mixed in the ratio Nb : Pd : Se, 2 : 1 : 5 (Nb powder, 99.99%, Johnson–Matthey; Pd powder, 99.95%, AESAR; Se powder, 99.999%, ATOMERGIC). This charge was heated at 1100 K for 288 hr in a sealed, evacuated silica tube. Small rod-shaped crystals up to 2 mm in length were dispersed in the tube. A chemical analysis was performed with

TABLE III

POSITIONAL PARAMETERS AND EQUIVALENT ISOTROPIC THERMAL PARAMETERS FOR $Co_2Ta_4PdSe_{12}$

Atom	Wyckoff notation	Site symmetry	x	y	z	B_{eq} (Å^2)
Co	4*i*	*m*	0.55051(2)	½	0.28261(11)	0.6
Ta(1)	4*i*	*m*	0.52526(6)	0	0.15041(3)	0.6
Ta(2)	4*i*	*m*	0.65983(6)	0	0.40630(3)	0.7
Pd	2*a*	2/*m*	0	0	0	1.0
Se(1)	4*i*	*m*	0.65202(15)	½	0.11771(9)	0.8
Se(2)	4*i*	*m*	0.48926(15)	½	0.60518(9)	0.8
Se(3)	4*i*	*m*	0.82068(14)	½	0.45051(9)	0.7
Se(4)	4*i*	*m*	0.41594(15)	0	0.23520(9)	0.8
Se(5)	4*i*	*m*	0.37924(15)	½	0.07342(9)	0.8
Se(6)	4*i*	*m*	0.68236(15)	0	0.28074(9)	0.7

the electron microprobe of an EDAX-equipped Cambridge S-4 scanning electron microscope. Analysis of the integrated intensities obtained from six crystals selected at random afforded the composition $Nb_{1.99(3)}Pd_{0.69(3)}Se_{5.02(5)}$.

Four-probe electrical conductivity measurements were made along the rod axis, *b*, of a single crystal, following procedures described previously (*21*).

The static magnetic susceptibility measurement was obtained with a S.H.E. VTS-10 SQUID susceptometer. The measurement was performed at 1 G with the sample contained in a closed silica bucket.

On the basis of Weissenberg and precession photographs, crystals of $Nb_2Pd_{0.71}Se_5$ were assigned to the Laue group 2/*m*. The systematic extinction, *hkl*, $h + k = 2n + 1$, is consistent with the space groups C_{2h}^3 – *C*2/*m*, C_s^3 – *Cm*, and C_2^3 – *C*2. After an absorption correction the equivalent reflections from the inner sphere of data were averaged in *C*2/*m* to yield a residual $R = 0.015$. Thus we favor the centrosymmetric group *C*2/*m*. The cell constants of $a = 12.788(6)$ Å, $b = 3.391(1)$ Å, $c = 15.416(6)$ Å, and $\beta = 101.48(2)°$ at 115 K were determined from a least-squares refinement of the setting angles of 15 reflections in the range $26° < 2\theta$ (Mo$K\alpha_1$) $< 39°$ on a Picker FACS-1 diffractometer.

Intensity data were collected with the θ–2θ scan technique and graphite-monochromated Mo$K\alpha$ radiation (*17*). Of the six standard reflections measured at 100-reflection intervals, only one reflection (020) showed a significant variation (11%) in intensity during the course of data collection. The variation resulted from movement of the crystal and was determined to be a function of the setting angle χ. As the remaining five standard reflections revealed no significant variation in intensity, those reflections with setting angle χ near that of the reflection (020) were eliminated from the data set. Crystal data and crystallographic details are provided in Table I.

All calculations were performed on a Harris 800 computer with programs standard in this laboratory. Inspection of a Patterson map revealed the positions of all the atoms except Nb(2) and Se(2). These atoms were located during subsequent electron density syntheses. In preparation for an absorption correction the partial occupancy of the Pd(2) site was determined during initial cycles of refinement. The final cycles of refinement were performed on F_0^2 with all 2359 unique reflections and included aniso-

TABLE IV

POSITIONAL PARAMETERS AND EQUIVALENT ISOTROPIC THERMAL PARAMETERS FOR $Nb_2Pd_{0.71}Se_5$

Atom	Wyckoff notation	Site symmetry	x	y	z	B_{eq} (Å^2)
Nb(1)	4*i*	*m*	0.076420(46)	½	0.179748(36)	0.5
Nb(2)	4*i*	*m*	0.152930(45)	0	0.377735(35)	0.4
Pd(1)	2*a*	2/*m*	0	0	0	0.4
Pd(2)[a]	2*c*	2/*m*	0	0	½	0.4
Se(1)	4*i*	*m*	0.350928(54)	0	0.489786(40)	0.4
Se(2)	4*i*	*m*	0.254444(52)	½	0.295556(39)	0.3
Se(3)	4*i*	*m*	0.176115(52)	0	0.097736(40)	0.4
Se(4)	4*i*	*m*	0.422897(53)	½	0.132039(40)	0.4
Se(5)	4*i*	*m*	0.500021(51)	0	0.322620(40)	0.4

[a] Occupancy = 0.419(3).

tropic thermal parameters for each atom and the occupancy for atom Pd(2). The final values for R and R_w on F_0^2 are 0.079 and 0.102, respectively. The final difference electron density map contains no features greater than 1.5% of the height of a Pd atom. An analysis of F_0^2 vs F_c^2 as a function of F_0^2, λ^{-1} sin θ, setting angles, and Miller indices reveals no unusual trends.

Final atomic parameters for $Nb_2Pd_{0.71}Se_5$ are provided in Table IV. Anisotropic thermal parameters and structure amplitudes are given in Tables S-V and S-VI,[1] respectively.

TABLE V

SELECTED BOND DISTANCES (Å) AND ANGLES (DEG.) FOR $Ta_2Pd_3Se_8$

Ta–2Se(1)	2.609(1)		
Ta–2Se(2)	2.611(1)	Se(1)–Ta–Se(1)	85.45(3)
Ta–1Se(3)	2.546(1)	Se(1)–Ta–Se(2)	75.64(2)
Ta–1Se(4)	2.552(1)	Se(1)–Ta–Se(4)	86.09(3)
Ta–2Pd(1)	3.393(1)	Se(3)–Ta–Se(4)	82.31(3)
Ta–2Pd(2)	2.907(1)		
Ta–2Ta	3.540(1)		
Pd(1)–2Se(1)	2.458(1)		
Pd(1)–2Se(2)	2.415(1)	Se(1)–Pd(1)–Se(2)	82.12(3)
Pd(1)–2Pd(1)	3.540(1)		
Pd(2)–2Se(3)	2.469(1)	Se(2)–Pd(2)–Se(3)	94.10(3)
Pd(2)–2Se(4)	2.470(1)	Se(3)–Pd(2)–Se(3)	91.61(4)
Pd(2)–1Se(2)	2.602(1)	Se(3)–Pd(2)–Se(4)	85.59(2)
Pd(2)–2Pd(2)	3.540(1)		

Results

$Ta_2Pd_3Se_8$. Selected bond distances and angles for the phase $Ta_2Pd_3Se_8$ are provided in Table V. A drawing of the structure is given in Fig. 3. The compound is isostruc-

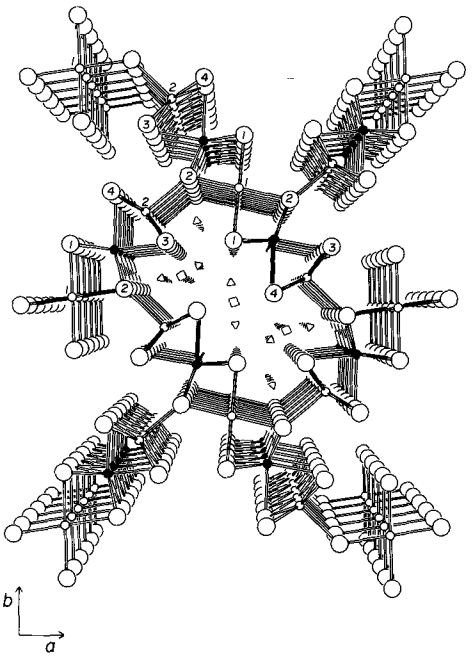

FIG. 3. Perspective view along [001] of the structure of $Ta_2Pd_3Se_8$. Ta atoms are small filled circles, Pd atoms are small open circles, Se atoms are large open circles.

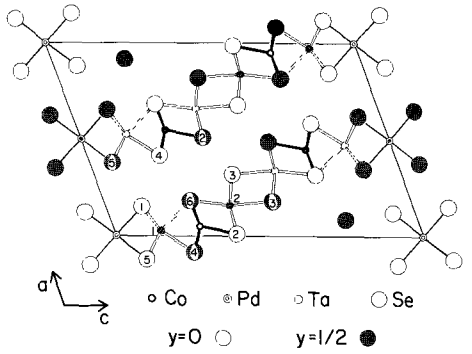

FIG. 4. Projection of the structure of $Co_2Ta_4PdSe_{12}$ onto the a–c plane showing the labeling scheme.

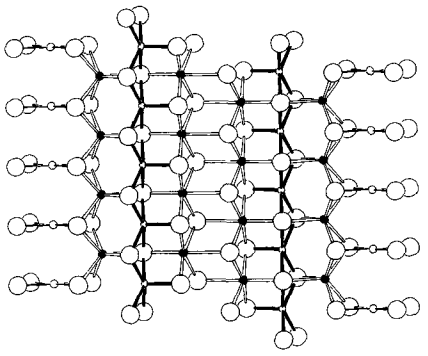

FIG. 5. Drawing of an individual layer of $Co_2Ta_4PdSe_{12}$ as viewed orthogonal to $(20\bar{1})$. Co atoms are small open circles with heavy bonds, Ta atoms are small filled circles, Pd atoms are small open circles with thin bonds, Se atoms are large open circles.

tural with $Nb_2Pd_3Se_8$ and a detailed description of that structure has been given previously (*16*). The metrical details parallel those of the phase $Nb_2Pd_3Se_8$; a consequence of the similar crystal radii (*22*) for the Ta and Nb atoms.

The Ta–Se and Pd(1)–Se distances exhibit little deviation from the corresponding interactions in the phase $Nb_2Pd_3Se_8$. The basal distances, Pd(2)–Se(3), 2.469(1) Å,[2] and Pd(2)–Se(8), 2.470(1) Å, of the square pyramid are somewhat shorter than the apical distance Pd(2)–Se(2), 2.602(1) Å. Atom Pd(2) rests 0.388(1) Å above the basal plane with the resultant angle Se(3)–Pd(2)–Se(4), 161.94(4)°. This angle is in satisfactory agreement with the theoretical value, 164°, for the C_{4v}-square pyramidal fragment ML_5 where M is a d^8 atom (*23*). The structural results for $Ta_2Pd_3Se_8$ then are consistent with the simple valence description: Ta^{V}, Pd^{II}, Se^{-II}.

$Co_2Ta_4PdSe_{12}$. A projection of the structure of $Co_2Ta_4PdSe_{12}$ with the labeling scheme is given in Fig. 4. The structure is a new laminar type with the layers extending parallel to $(20\bar{1})$. A drawing of an individual layer as viewed orthogonal to $(20\bar{1})$ is provided in Fig. 5. The slab, in part topologically similar to the structural units of $Ta_2Pd_3Se_8$, is composed of an unusual association of metal-centered polyhedra. A chain of face-to-face square planes of Se atoms occupied by the Pd atoms bridges two columns of edge-sharing trigonal prisms centered by the Ta(1) atoms. The quadrilateral faces derived from the Se atoms of adjacent trigonal prisms form the basal planes for the column of edge-sharing square pyramids occupied by the Co atoms. This combination of polyhedra parallels that of the material $Ta_2Pd_3Se_8$. The layer $Co_2Ta_4PdSe_{12}$ is completed with introduction of the double chain of edge-sharing Se octahedra occupied by the Ta(2) atoms (Fig. 5). As shown in Fig. 6, the full nature of the structure is realized by a pseudo-closest packing of these buckled layers.

Metrical data for the structure of $Co_2Ta_4PdSe_{12}$ are provided in Table VI. The average Pd–Se distance, 2.440(9) Å, is comparable with that observed in $Ta_2Pd_3Se_8$, 2.44(2) Å, and is in agreement with the value predicted from crystal radii (*22*). The square plane shortens along the edge shared with the trigonal prism resulting in the acute angle Se(1)–Pd–Se(5), 86.17(6)°.

The apical Co–Se distance, 2.392(3) Å, is intermediate to those of the basal plane,

[2] An estimated standard deviation in parentheses is the larger of that estimated for a single observation from the inverse matrix or from the values averaged.

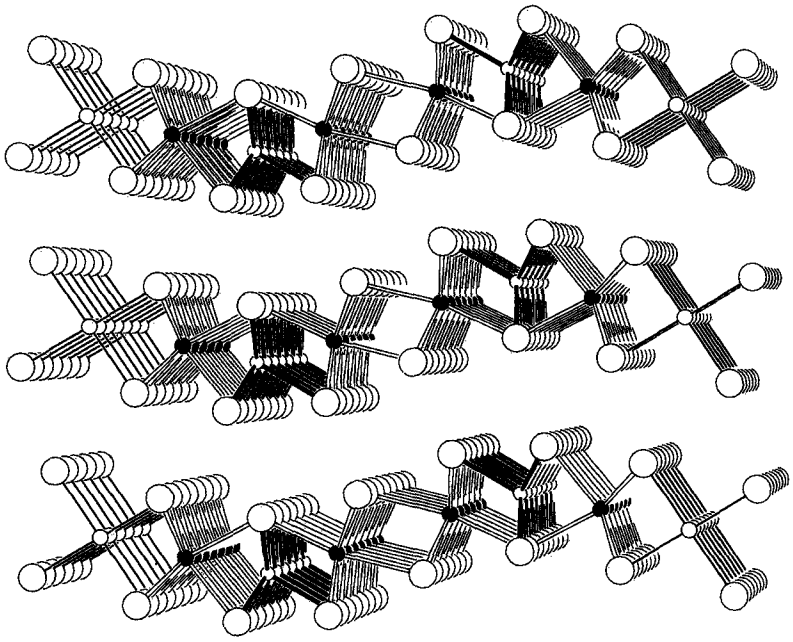

FIG. 6. Perspective view along [010] of the structure of $Co_2Ta_4PdSe_{12}$. Co atoms are small open circles with heavy bonds, Ta atoms are small filled circles, Pd atoms are small open circles with thin bonds; Se atoms are large open circles.

TABLE VI

SELECTED BOND DISTANCES (Å) AND ANGLES (DEG.) FOR $Co_2Ta_4PdSe_{12}$

Co–2Se(4)	2.382(2)		
Co–2Se(6)	2.423(2)		
Co–1Se(2)	2.392(3)		
Co–2Ta(2)	2.872(2)	Se(2)–Co–Se(4)	89.30(8)
Co–2Ta(1)	2.989(2)	Se(2)–Co–Se(6)	112.84(8)
Co–2Co	3.413(1)	Se(4)–Co–Se(4)	91.49(10)
Ta(1)–2Se(1)	2.593(2)	Se(1)–Ta(1)–Se(1)	82.29(6)
Ta(1)–1Se(4)	2.508(2)	Se(1)–Ta(1)–Se(5)	79.94(5)
Ta(1)–2Se(5)	2.595(2)	Se(1)–Ta(1)–Se(6)	83.53(5)
Ta(1)–1Se(6)	2.626(2)	Se(4)–Ta(1)–Se(5)	84.74(5)
Ta(1)–2Pd	3.281(1)	Se(4)–Ta(1)–Se(6)	78.55(6)
Ta(1)–2Ta(1)	3.413(1)		
Ta(2)–2Se(2)	2.528(2)	Se(2)–Ta(2)–Se(2)	84.90(6)
Ta(2)–2Se(3)	2.597(2)	Se(2)–Ta(2)–Se(3)	94.95(4)
Ta(2)–1Se(3)	2.683(2)	Se(2)–Ta(2)–Se(6)	104.75(5)
Ta(2)–1Se(6)	2.537(2)	Se(3)–Ta(2)–Se(3)	82.17(6)
Ta(2)–2Ta(2)	3.413(1)	Se(3)–Ta(2)–Se(6)	88.14(5)
		Se(6)–Ta(2)–Se(3)	168.75(6)
Pd–2Se(1)	2.432(2)		
Pd–2Se(5)	2.448(2)	Se(1)–Pd–Se(5)	86.17(6)
Pd–2Pd	3.413(1)		

2.382(2) and 2.423(2) Å. This may be contrasted with the square pyramid in $Ta_2Pd_3Se_8$ where the apical Pd(2)–Se(2) distance is longer than the distances of the basal plane (Table V). Although the Co–Se distances of the pyramid are fairly regular, the angles Se(2)–Co–Se(6), 112.84(8)°, and Se(2)–Co–Se(4), 89.30(8)°, and the distances Se(2)–Se(4), 3.355(2) Å, and Se(2)–Se(6), 4.051(3) Å, demonstrate the highly distorted nature of this polyhedron. The Co atom rests 0.468(2) Å above the basal plane. Although five-coordinate Co atoms are a common feature in molecular compounds (*24, 25*), the stereochemistry about Co in solid-state chalcogenides has been dominated by tetrahedral (*26*) and octahedral environments (*27–29*). Insofar as we know this is the first clearly established occurrence of a Co atom in a square-pyramidal environment of chalcogen atoms in a solid-state inorganic material.

The Ta(1)–Se distances in the trigonal

TABLE VII

SELECTED BOND DISTANCES (Å) AND ANGLES (DEG.) FOR $Nb_2Pd_{0.71}Se_5$

Pd(1)–2Se(3)	2.448(1)		
Pd(1)–2Se(4)	2.432(1)	Se(3)–Pd(1)–Se(4)	87.79(4)
Pd(1)–2Pd(1)	3.391(1)		
Pd(2)–4Se(1)	2.533(1)	Se(1)–Pd(2)–Se(1)	84.05(4)
Nb(1)–1Se(2)	2.599(1)	Se(2)–Nb(1)–Se(3)	83.49(3)
Nb(1)–2Se(3)	2.596(1)	Se(2)–Nb(1)–Se(5)	80.93(4)
Nb(1)–2Se(4)	2.588(1)	Se(3)–Nb(1)–Se(3)	81.55(3)
Nb(1)–1Se(5)	2.581(1)	Se(3)–Nb(1)–Se(4)	81.49(4)
Nb(1)–2Nb(1)	3.391(1)	Se(4)–Nb(1)–Se(4)	81.88(4)
		Se(4)–Nb(1)–Se(5)	81.25(3)
Nb(2)–2Se(1)	2.662(1)	Se(1)–Nb(2)–Se(1)	79.11(4)
Nb(2)–1Se(1)	2.766(1)	Se(1)–Nb(2)–Se(2)	79.71(4)
Nb(2)–2Se(2)	2.612(1)	Se(1)–Nb(2)–Se(5)	80.34(4)
Nb(2)–2Se(5)	2.600(1)	Se(2)–Nb(2)–Se(2)	80.97(4)
Nb(2)–2Nb(2)	3.391(1)	Se(2)–Nb(2)–Se(5)	80.34(4)
		Se(5)–Nb(2)–Se(5)	81.41(4)

prism range from 2.508(2) to 2.626(2) Å and the average, 2.59(4) Å, is comparable with that observed in $Ta_2Pd_3Se_8$, 2.59(3) Å, and 2H–$TaSe_2$, 2.59(1) Å (*30*). The Ta(2)–Se distances in the octahedron range from 2.528(2) to 2.683(2) Å and the average 2.58(6) Å is consistent with that observed in 4H–$TaSe_2$, 2.58(2) Å (*30*). The Ta(2) atoms are displaced by 0.294(1) Å from the plane defined by the atoms Se(2)–Se(2)–Se(3). The displacement is away from the common edge of the bioctahedron toward the edge shared with the square pyramid.

The occurrence of trigonal prismatic and octahedral coordination of Ta atoms by chalcogen in one phase has already been demonstrated in $TaSe_2$ (*31*). The environment about the Ta atom is trigonal prismatic below 1065 K and octahedral above 1135 K, whereas at intermediate temperatures the two types of coordination coexist. This behavior clearly demonstrates that octahedral coordination is entropically favored (*32*). Additional models that involve electronic factors (*32, 33*) or plots (*34*) of radius ratios vs fractional ionic character have been advanced as explanations for the preference of a given metal atom for an octahedral or trigonal prismatic geometry. For the present material, the coexistence of the two types of polyhedra may derive in part from nonequal formal oxidation states of the two types of Ta atoms. Such a formulation is consistent with the reported models although the interaction of all the atoms must be a consideration in satisfying the topological requirements for formation of the three-dimensional structure.

Each Se atom is bonded to three metal atoms, except atom Se(6) which is bound to four metal atoms. The Se–Se distances within a layer range from 3.251(3) to 4.051(3) Å. Hence there are no short Se–Se distances indicative of Se–Se bonding. As compared with the Se · · · Se distance 3.43 Å across the van der Waals' gap of 2H–$TaSe_2$ (*30*), the gap of the present material affords a broad range of Se · · · Se distances, 3.380(3) to 4.364(4) Å. These distances reflect the substantial distortions of the vacant octahedral and tetrahedral sites between the layers of the structure.

All the metrical details appear to be consistent with the rather remarkable ordered string of metal atoms (Pd–Ta–Co–Ta–Ta–Co–Ta–Pd) where the Pd–Pd separation is greater than 22 Å! This arrangement is further supported by the satisfactory agreement of the calculated X-ray powder diffraction pattern with that obtained from a

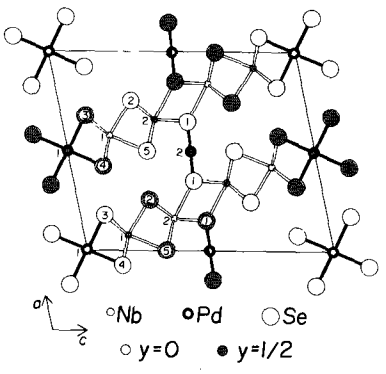

FIG. 7. Projection of the structure of $Nb_2Pd_{0.71}Se_5$ onto the *a–c* plane showing the labeling scheme.

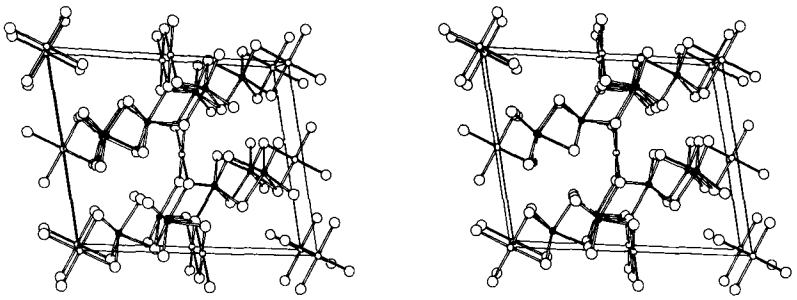

FIG. 8. Stereoview of the structure of $Nb_2Pd_{0.71}Se_5$ as viewed along [010]. Nb atoms are small filled circles, Pd atoms are small open circles, Se atoms are large open circles.

powder prepared from a stoichiometric combination of the elements.

$Nb_2Pd_{0.71}Se_5$. Like the material $Co_2Ta_4PdSe_{12}$, the phase $Nb_2Pd_{0.71}Se_5$ forms with a new laminar structural type. This phase is one member of a set of structurally related Nb–Pd–Se phases derived from Nb_2PdSe_6 (*34*); the other members of this set will be discussed in forthcoming articles.

Selected bond distances and angles for $Nb_2Pd_{0.71}Se_5$ are given in Table VII. A projection of the structure onto the *a–c* plane with the labeling scheme is given in Fig. 7. A stereoview of the structure is provided in Fig. 8.

The structure consists of slabs of composition $^2_\infty[Nb_4PdSe_{10}]$ extending parallel with $(20\bar{1})$. A drawing of an individual slab as viewed orthogonal to $(20\bar{1})$ is furnished in Fig. 9. The slabs may be described as associated columns of square-planar and trigonal-prismatic polyhedra of Se atoms. The atoms Pd(1) center a column of face-to-face square planes and the atoms Nb(1) center a column of edge-sharing trigonal prisms. The remaining metal atoms, Nb(2), occupy a chain of face-sharing trigonal prisms. These independent columns link exclusively through edge sharing of the polyhedra. Adjacent units of Nb_4PdSe_{10} undergo relative translations of *b*/2 thus completing an unprecedented distorted monocapped trigonal-prismatic environment of chalcogenide atoms about the atoms Nb(2). The relative disposition of these units is emphasized by the dashed lines in Fig. 9. As shown in Fig. 10, the full nature of the structure is realized with a pseudo-closest packing of the layers in the manner, ABAB . . . , and insertion of the statistically distributed atoms Pd(2) in the square-planar sites.

The average Pd(1)–Se distance, 2.439(9) Å, is comparable with that of similar materials containing Pd atoms bound to Se atoms in a square-planar manner; $Nb_2Pd_3Se_8$

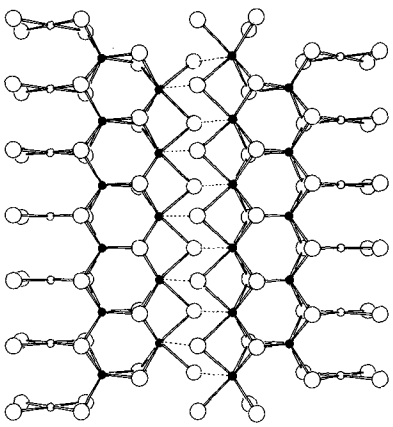

FIG. 9. Drawing of a layer $[Nb_4PdSe_{10}]_\infty$ as viewed orthogonal to $(20\bar{1})$. Nb atoms are small filled circles, Pd atoms are small open circles, Se atoms are large open circles.

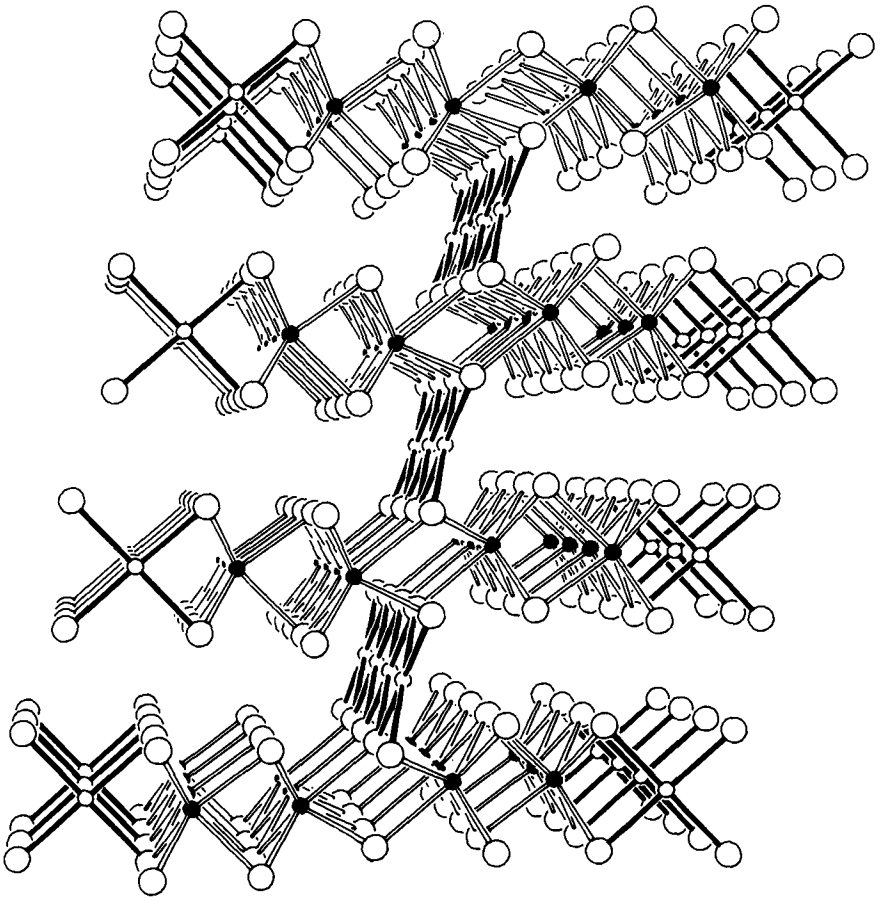

FIG. 10. Perspective view of $Nb_2Pd_{0.71}Se_5$ as viewed along [010]. Nb atoms are small filled circles, Pd atoms are small open circles, Se atoms are large open circles.

(*16*), 2.44(2) Å, and $PdSe_2$ (*35*), 2.44 Å. Similarly the average Nb(1)–Se distance, 2.592(7) Å, is consistent with that observed in $NbSe_2$, 2.595(2) Å (*36*), and $Nb_2Pd_3Se_8$, 2.60(3) Å (*16*). The prism about the atom Nb(2) is less regular with distances Nb(2)–Se(1), 2.662(1) Å; Nb(2)–Se(2), 2.612(1) Å; and Nb(2)–Se(5), 2.600(1) Å. The Nb(2)–Se(1) capping distance, 2.766(1) Å, is comparable with similar interactions in other Nb–Se materials (*37*).

The atoms Se(2)–Se(5) are bonded to three metal atoms; atom Se(1) bonds to three Nb atoms and the statistically distributed Pd(2) atoms. There are no indications of Se–Se bonding, as the Se–Se distances within a slab range from 3.131(1) to 3.459(1) Å. The Se · · · Se distances between the sheets range from 3.516(2) to 3.627(2) Å. These values are comparable with the Se · · · Se distances across the van der Waals' gap of $NbSe_2$, 3.550(4) Å (*36*). Like that gap in $NbSe_2$, between the sheets of $^2_\infty[Nb_4PdSe_{10}]$ in the present structure there are several vacant octahedral and tetrahedral sites. In addition, atoms Se(1) and Se(5) from adjacent slabs form a distorted rhombic prism. The rhombus is 42% occupied by the Pd(2) atoms and the resultant Pd(2)–Se(1) distance, 2.533(1) Å, is long.

Insofar as we know this is the first example of such a coordination site between the slabs of a layered chalcogenide.

A plot of the electrical conductivity data over the temperature range 285–110 K is provided in Fig. 11. The behavior is that expected for a metallic conductor. A transition to the superconducting state was not observed from a magnetic susceptibility measurement performed over the temperature range 20–4 K. The electrical conductivity is consistent with the observed nonstoichiometric nature of the material and assignment of nonintegral formal oxidation states for the Nb atoms. The phase $Nb_2Pd_{0.71}Se_5$ may be viewed in a manner analogous to the layered dichalcogenides with the slabs $^2_\infty[Nb_4PdSe_{10}]$ in $Nb_2Pd_{0.71}Se_5$ corresponding, for example, to the $^2_\infty[NbSe_2]$ slabs in $NbSe_2$. If we assume the partial valence description, Pd^{II}, Se^{II-}, the metallic behavior of $Nb_2Pd_{0.71}Se_5$ derives as in $NbSe_2$ from the partially filled *d*-like band associated with the Nb atoms. In addition, this partially filled band serves as a sink for charge transfer, thus forming the basis of the observed insertion (intercalation) chemistry (*2*). Indeed, results of chemical analyses and X-ray powder diffraction measurements indicate that the concentration of Pd atoms between the slabs $^2_\infty[Nb_4PdSe_{10}]$ may be varied (*34*). The variation has further been demonstrated from a single-crystal X-ray study of the material $Ta_2Pd_{0.91}S_5$ (*38*), which is isostructural with $Nb_2Pd_{0.71}Se_5$.

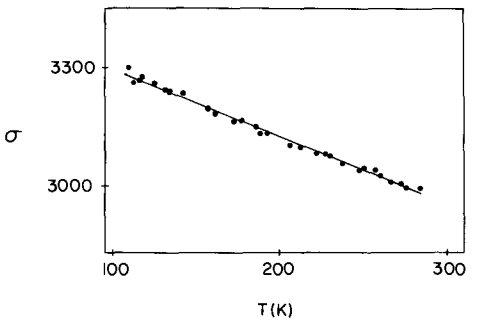

FIG. 11. Electrical conductivity (ohm^{-1} cm^{-1}) vs temperature as measured along the needle axis, *b*, for the material $Nb_2Pd_{0.71}Se_5$.

The structure of the present material marks an additional departure (cf. $Nb_2Pd_3Se_8$) from the known ternary transition-metal Nb chalcogenides that form as polychalcogenides or as insertion compounds of the layered $NbSe_2$ structural type. The thermodynamic stability of the present material probably arises in good measure from the high formal charge of the Nb atoms and the increased bonding energy associated with the seven-coordinate Nb(2) atoms. The very existence of this material as well as those previously described derives from the satisfaction of the stereochemical preferences of the metal atoms in an efficient packing of Se atoms. As well as the interesting structural features about the metal atoms, the presence of relatively high formal oxidation states and several vacant sites presents a number of possibilities for further chemical manipulation and substitution; some of these aspects will appear in forthcoming publications.

Acknowledgments

This work was supported by the U.S. National Science Foundation—Solid State Chemistry—Grant DMR-83-15554. Some of the measurements were carried out in the Magnet, SEM, and X-ray Facilities of Northwestern University's Materials Research Center, supported in part under the NSF-MRL program (Grant DMR82-16972). Shang Maoyu thanks Academic Sinica and the U.S.–China program of the National Science Foundation (Grant INT-81-17267) for support.

References

1. J. A. WILSON AND A. D. YOFFE, *Adv. Phys.* **18,** 193 (1969).
2. "Physics and Chemistry of Materials with Layered Structures" (F. Lévy, Ed.), Reidel, Dordrecht (1979).
3. S. S. P. PARKIN AND R. H. FRIEND, *Philos. Mag. B* **41,** 65, 95 (1980).

4. S. S. P. PARKIN AND A. R. BEAL, *Philos. Mag. B* **42,** 627 (1980).
5. F. R. GAMBLE, F. J. DISALVO, R. A. KLEMM, AND T. H. GEBALLE, *Science* **168,** 568 (1970).
6. F. R. GAMBLE, J. H. OSIECKI, M. CAIS, R. PISHARODY, F. J. DISALVO, AND T. H. GEBALLE, *Science* **174,** 493 (1971).
7. J. RIJNSDORP AND F. JELLINEK, *J. Solid State Chem.* **25,** 325 (1978).
8. D. E. MONCTON, J. D. AXE, AND F. J. DISALVO, *Phys. Rev. B* **16,** 801 (1977).
9. R. BROUWER AND F. JELLINEK, *Physica B* **99,** 51 (1980).
10. C. F. VAN BRUGGEN, C. HAAS, AND G. A. WIEGERS, *J. Solid State Chem.* **27,** 9 (1979).
11. A. R. BEAL, *in* "Physics and Chemistry of Materials with Layered Structures" (F. Lévy, Ed.), Vol. 6, p. 251, Reidel, Dordrecht (1979).
12. S. J. HILLENIUS, R. V. COLEMAN, R. M. FLEMING, AND R. J. CAVA, *Phys. Rev. B* **23,** 1567 (1981).
13. R. J. CAVA, V. L. HIMES, A. D. MIGHELL, AND R. S. ROTH, *Phys. Rev. B* **24,** 3634 (1981).
14. A. MEERSCHAUT, P. GRESSIER, L. GUEMAS, AND J. ROUXEL, *Mater. Res. Bull.* **16,** 1035 (1981).
15. A. BEN SALEM, A. MEERSCHAUT, L. GUEMAS, AND J. ROUXEL, *Mater. Res. Bull.* **17,** 1071 (1982).
16. D. A. KESZLER AND J. A. IBERS, *J. Solid State Chem.* **52,** 73 (1984).
17. J. M. WATERS AND J. A. IBERS, *Inorg. Chem.* **16,** 3273 (1977).
18. D. T. CROMER AND J. T. WABER, "International Tables for X-Ray Crystallography," Vol. IV, Table 2.2A; D. T. Cromer, Table 2.3.1, Kynoch Press, Birmingham, England (1974).
19. J. A. IBERS AND W. C. HAMILTON, *Acta Crystallogr.* **17,** 781 (1964).
20. B. A. FRENZ, *in* "Computing in Crystallography" (H. van Konigsveld and G. C. Bassi, Eds.), p. 64, Delft Univ. Press, Delft, Holland (1983).
21. T. E. PHILLIPS, R. P. SCARINGE, B. M. HOFFMAN, AND J. A. IBERS, *J. Amer. Chem. Soc.* **102,** 3435 (1980).
22. R. D. SHANNON, *in* "Structure and Bonding in Crystals" (M. O'Keeffe and A. Navrotsky, Eds.), Vol. 2, p. 53, Academic Press, New York (1981).
23. A. R. ROSSI AND R. HOFFMANN, *Inorg. Chem.* **14,** 365 (1975).
24. B. A. COYLE AND J. A. IBERS, *Inorg. Chem.* **9,** 767 (1970).
25. J. K. STALICK, P. W. R. CORFIELD, AND D. W. MEEK, *Inorg. Chem.* **12,** 1668 (1973).
26. F. BOHM, F. GRØNVOLD, H. HARALDSEN, AND H. PRYDZ, *Acta Chem. Scand.* **9,** 1510 (1955).
27. V. S. TENGNÉR, *Z. Anorg. Allg. Chem.* **239,** 126 (1938).
28. S. FURUSETH AND A. KJEKSHUS, *Acta Chem. Scand.* **23,** 2325 (1969).
29. K. ANZENHOFER AND J. J. DE BOER, *Acta Crystallogr. Sect. B* **25,** 1419 (1969).
30. B. E. BROWN AND D. J. BEERNSTEN, *Acta Crystallogr.* **18,** 31 (1965).
31. R. HUISMAN AND F. JELLINEK, *J. Less-Common Met.* **17,** 111 (1969).
32. R. HUISMAN, R. DEJONGE, C. HAAS, AND F. JELLINEK, *J. Solid State Chem.* **3,** 56 (1971).
33. M. KERTESZ AND R. HOFFMANN, *J. Amer. Chem. Soc.* **106,** 3453 (1984).
34. D. A. KESZLER, Ph.D. dissertation, Northwestern University, 1984.
35. F. GRØNVOLD AND E. RØST, *Acta Crystallogr.* **10,** 329 (1957).
36. M. MAREZIO, P. D. DERNIER, A. MENTH, AND G. W. HULL, JR., *J. Solid State Chem.* **4,** 425 (1972).
37. A. MEERSCHAUT AND J. ROUXEL, *J. Less-Common Met.* **39,** 197 (1975).
38. P. J. SQUATTRITO AND J. A. IBERS, unpublished results.